Optimized Magnetics and Improved Power Devices Utilization for PV Modules by Using Hybrid Transformer ZVS/ZCS Dc-Dc Converter

Challa Srinivas Reddy
Bachelor of Technology(EEE),
Master of Technology (PEED), PGDC in T&D,
Arjun College of Technology and Sciences,
(Hyderabad).

Rosaiash Mudigondla
M.Tech (PEED),
Assistant Professor,
Arjun College of Technology & Sciences.

Abstract:

The implementation converter utilizes a hybrid transformer to incorporate the resonant operation mode into a traditional high boost ratio active-clamp coupled-inductor pulse-width-modulation dc– dc converter, High boost ratio dc–dc converter with the application for photovoltaic (PV) modules. achieving zero-voltage-switching (ZVS) turn-on of active switches and zero-current-switching turn-off of diodes. As a result of the inductive and capacitive energy being transferred simultaneously within the whole switching period, power device utilization (PDU) is improved and magnetic utilization (MU) is optimized. The improved PDU allows reduction of the silicon area required to realize the power devices of the converter

Technology used:

- High CEC efficiency,
- hybrid transformer,
- improved power device utilization (PDU),
- low device voltage stresses,
- optimized magnetic utilization (MU),
- PV modules.

Exciting system:

The optimized MU reduces the dc-bias of magnetizing current in the magnetic core, leading to smaller sized magnetics. Since the magnetizing current has low dc-bias, the ripple magnetizing current can be utilized to assist ZVS of main switch, while maintaining low rootmean-square (RMS) conduction loss. The voltage stresses on the active switches and diodes are maintained at a low level and are independent of the wide changing PV voltages as a result of the resonant capacitor in series in the energy transfer loop.

INTRODUCTION:

GLOBAL demand for electrical energy is constantly increasing. Due to the declining production and the rising cost of nonrenewable energy supplies, there has been a growing demand for the utilization of renewable energy sources. Among these renewable energy sources, photovoltaic (PV) energy has experienced remarkable growth over the past decades. The PV energy generated from sunlight is captured by dc PV modules. The power generated by these modules is integrated into the existing ac power distribution infrastructure through the power conditioners [1]–[3], which can adopt two-stage or singlestage system configurations. Compared to single-stage systems, the two-stage single-phase

architecture can use the high-voltage dc-bus as double-line ripple power buffer to avoid failure-prone electrolyte capacitors [4]–[6]. In two-stage PV power conditioners, high boost ratio dc–dc converters are used to increase the low PV voltage to a high dc voltage to interface the PV modules with either a low-power individual inverter or a high power centralized grid-connected inverter [1]–[3]. Since galvanic insulation is not mandatory in code, this high boost ratio dc–dc converter can be isolated or nonisolated [1], [4]–[8].

Fig. 1 shows a cluster of I–V curves based on datasheet of a 240-W PV module CS6P-240P from CanadianSolar [9] at different irradiance levels and environmental temperatures. Due to the different output voltage and power from the PV panel, it would be beneficial to have a high boost ratio dc–dc converter with a high efficiency over the entire PV voltage and output power ranges to maximize energy yield during different operating conditions. Another requirement for this high boost ratio dc–dc converter is to have high power density and low profile to integrate with the PV modules. With the PV module costs continuously dropping, the electrics cost is becoming increasingly dominant. This requires that the dc–dc converter to have simple structure and low electronic cost.

Of the high boost ratio dc–dc converter topologies presented [6], [8]–[27], the uses of coupled-inductor are attractive due to the fact that only one magnetics is required and low voltage active switches can be utilized. The reason that the primary side active switches of the high boost ratio converters have low voltage stress comes from the transformer effect of the coupledinductors. Since the primary active switches have low voltage stresses, the circuits can use low voltage MOSFETs that generally have a low Rds(on) and fast switching speed, decreasing both the conduction and switching losses. To further reduce the switching losses, active-clamp techniques have been widely used [19], [24], [27]–[29], A zero-voltage-switching (ZVS) high boost ratio active-clamp

coupled-inductor (ACCI) converter, as shown in Fig. 2(b), was presented in [19].

This converter could be derived from traditional active-clamp flyback converter [28], [29], as shown in Fig. 2(a), by splitting secondary side and series connecting the output winding with the clamping capacitor Cc . Besides inheriting the simple structure, low voltage stresses and ZVS operation of active switches, the boost ratio of this converter was increased. This allows designing coupledinductor with lower turns ratio, which reduces the primary-side root-mean-square (RMS) conduction losses.

As a result of increased boost ratio, the voltage stresses of the active switches were reduced, allowing use of low-voltage MOSFET switches with low Rds(on). However, voltage stress on the output diode of ACCI converter is still high as that of traditional active-clamp flyback converter. To reduce voltage ringing across the output diode, a passive snubber was added [19], which degraded the efficiency of the converter. Similar to traditional active-clamp flyback converter, the ACCI converter only transfers energy to the secondary side during the interval when the main switch is off, causing poor magnetic utilization (MU) and high dc-bias magnetizing current.

In order to avoid high ripple current, the energy stored in the leakage and/or external inductors instead of energy in magnetizing inductance [19], [28]–[29] has been utilized to achieve ZVS of main switch. However, a large leakage or external inductance results in a loss of effective duty cycle on the secondary side of coupled-inductor. Normally, a transformer with higher turns ratio is required to compensate the secondary-side duty loss. With a higher turns ratio, the reflected output current into the primary side is increased, which results in higher primary-side conduction losses. Besides, the higher turns ratio increases the voltage stress of the output diode. The conflict between low conduction losses and low switching losses prevented this converter to achieve high efficiency over wide power range.

This is not desirable for PV module power conversion where the high efficiency over a wide power is required because the performance is weighted differently for specific power levels in the California Energy Commission (CEC) or European Union (EU) standards.
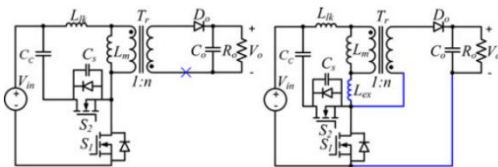

Fig. 2. (a) Active-clamp flyback converter. (b) Active-clamp coupled-inductor high boost ratio converter.

In this paper, a high boost ratio ZVS/ZCS dc–dc converter with hybrid transformer [6], [30] is presented to achieve high system level efficiency over wide input voltage and power ranges. By adding a small resonant capacitor and a resonant diode into the previous ACCI converter [19], a hybrid operation mode [6], [30] which combines pulse-width-modulation (PWM) and resonant power conversions, is introduced into the proposed high boost ratio converter. This converter utilizes a hybrid transformer that combines the modes where the transformer operates under normal conditions and where it operates as a coupled-inductor to transfer the energy to high voltage side improving the utilization of the magnetic core. The dc-bias of the magnetizing current can be effectively reduced and smaller sized magnetics can be utilized.

Due to the low dc-bias of the magnetizing current the proposed converter can be designed with small magnetizing inductance allowing bidirectional magnetizing current flow to achieve ZVS of main switch while maintaining low RMS conduction loss. The output diodes in the proposed converter can achieve zero-current-switching (ZCS) turn-off because the resonant currents resonate back to zero at the switching transitions. The continuous input current with combined sinusoidal resonant and linear PWM current leads to smaller current ripple and reduced

RMS conduction losses. The voltage stresses on the active switches and diodes are maintained at a low level and are independent of the wide changing input PV voltages as a result of the resonant capacitor in series in the energy transfer loop.

Due to reduced switching losses achieved by ZVS and ZCS operations and reduced RMS conduction losses, the proposed converter can achieve high system efficiency over wide input voltage and power ranges. The performance of the proposed converter was verified experimentally utilizing a 250-W prototype circuit with the PV module voltages from 20 to 45 V. Experimental results indicate that the specific input voltage ranges within which the proposed converter has highest CEC efficiencies match the maximum power point ranges of I–V curves of PV module datasheet, which ensures maximum energy yield from the PV modules.

PROPOSED CONVERTER TOPOLOGY

Fig. 3 shows the circuit diagram of the proposed converter. HT is a hybrid transformer with primary to secondary turns ratio 1:n and with secondary-reflected equivalent leakage inductance Llk ; S1 is the main switch and S2 is the auxiliary active-clamp switch; Cc is the clamping capacitor; Dr is a resonant diode, which provides a unidirectional current flow path to charge the resonant capacitor Cr when S1 is on; Do is the output diode; Cj represents the equivalent parasitic junction capacitors of MOSFETs, Cs is the equivalent capacitor of the diodes Do and Dr , Co is the output capacitor; Ro is the equivalent resistive load, and Vin represents PV-side equivalent voltage.

Fig. 4 illustrates the eight steady-state topological states of the proposed converter within one switching cycle. Fig. 5 shows the key voltage and current waveforms for specific devices over one switching cycle. In Fig. 5, g1 and g2 represent the driver signals to S1 and S2 and the definition of other notations is represented in Fig. 3.

OPERATION ANALYSIS

For the description of the circuit operation and for the subsequent design procedure in the followed sections, the following assumptions are made:

1) Ideal MOSFET switches S1 and S2 with body diodes;

2) D is the steady-state duty ratio based on S1;

3) The voltage ripples on Co and Cc are negligibly small.

The sequence of topological states is described as below. t0 –t1 : At t0 , S2 is turned off. The negative magnetizing current iLm starts to charge Cj . Due to the voltage potential change
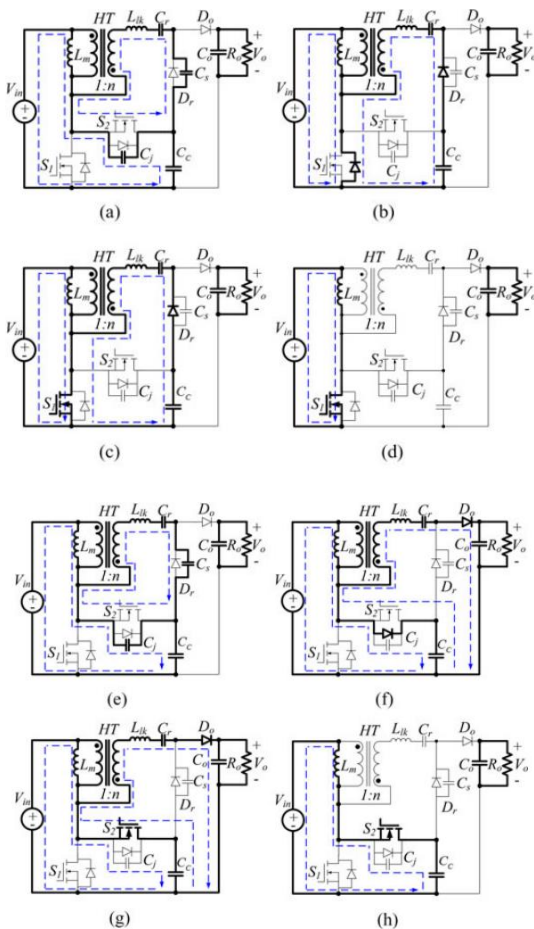
Fig.4. Topological stages: (a) t0-t1, (b) t1-t2, (c) t2-t3, (d) t3-t4, (e) t4-t5, (f) t5-t6, (g) t6-t7, and (h) t7-t8.

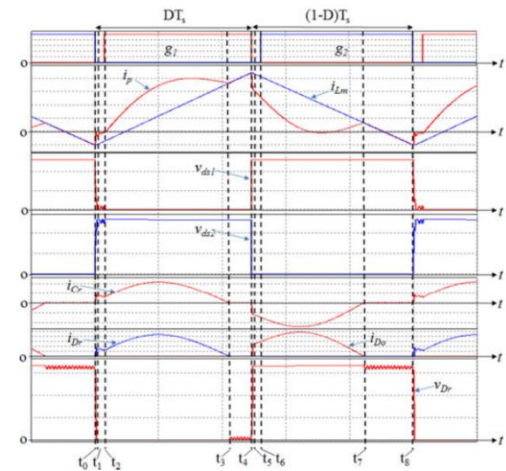**Fig. 5.Steady-state waveforms.**

Operation of modes:

Mode 1 t1 –t2:

At t1 , vds1 is reduced to zero. is1 , which is equal to the sum of ip and niC r , flows through the body diode of S1 . This provides a ZVS condition for S1 .Vin is applied on Lm and iLm is linearly increased. Meanwhile, the secondary-reflected input voltage nVin along with VC c charge Cr in a resonant manner through the resonant loop including secondary side of HT, Llk , Cr , Dr , Cc and body diode of S1 .

Mode2: t2 –t3 :

At t2 , S1 is turned on with ZVS. The state equations of secondary resonant circuit from t1 to t3 can be written as follows:

$$L_{lk} \frac{\mathrm{d}i_{Cr}}{\mathrm{d}t} = nV_{\mathrm{in}} + V_{Cc} - v_{Cr} \qquad (1)$$

$$C_r \frac{\mathrm{d}v_{Cr}}{\mathrm{d}t} = i_{Cr} \qquad (2)$$

From (1) and (2), iC r and vC r can be calculated as

$$i_{Cr}(t) = \frac{nV_{\mathrm{in}} + V_{Cc} - v_{Cr}(t_1)}{Z_{r1}} \sin \omega_{r1}(t - t_1) \qquad (3)$$

$$v_{Cr}(t) = nV_{\mathrm{in}} + V_{Cc}$$
$$- (nV_{\mathrm{in}} + V_{Cc} - v_{Cr}(t_1)) \cos \omega_{r1}(t - t_1) \qquad (4)$$

Where Zr1 and ωr1 are the angular resonant frequency and impedance given by Zr1 = Llk /Ceq1 ,ωr1 = 1/LlkCeq1 ,

Ceq1 = Cr Cc (Cr +Cc) ≈ Cr (Cc Cr).

Mode 3: t3 –t4:

At t3 ,iDr resonates back to zero so Dr turns off with ZCS. Vin continues to linearly charge Lm . From t1 to t4 ,iLm is linearly charged by Vin and is given by

$$i_{L_m}(t) = i_{L_m}(t_1) + \frac{V_{in}}{L_m}(t - t_1) \qquad (5)$$

Mode 4:t4 –t5:

At t4 , S1 is turned off. iLm starts to discharge Cj . Due to the voltage potential change of the drain node of S1 , a parasitic minor resonant loop composed of secondary side of HT, Llk , Cr , Cs , and Cj starts to resonate.

Mode 5:t5 –t6:

At t5 , Cs is discharged to the point where the antiparallel diode of S2 starts to conduct. This provides ZVS turn-on of S2 . Also, the voltage potential of anode of Do increases high enough leading Do to be forward-biased.

Mode 6: t6 –t7:

At t6 , S2 is turned on with ZVS. Since it takes a long time interval before iLm reduces to zero, ZVS of S2 is easily achieved. The energy is transferred to the output with the resonant current iDo . The state equations of secondary resonant circuit from t5 to t7 can be written as follows:

$$L_{lk}\frac{di_{Cr}}{dt} = n(V_{in} - V_{Cc}) + V_o - V_{Cc} - v_{Cr} \qquad (6)$$

$$C_r\frac{dv_{Cr}}{dt} = i_{Cr} \qquad (7)$$

From (6) and (7), iC r and vC r can be calculated as

$$i_{Cr}(t) = \frac{nV_{in} - (n+1)V_{Cc} + V_o - v_{Cr}(t_7)}{Z_{r2}}\sin\omega_{r2}(t - t_5) \qquad (8)$$

$$v_{Cr}(t) = nV_{in} - (n+1)V_{Cc} + V_o - (nV_{in} - (n+1)V_{Cc} + V_o - v_{Cr}(t_7))\cos\omega_{r2}(t - t_5) \qquad (9)$$

Where Zr2 = Llk /Ceq2 ,ωr2 = 1/LlkCeq2 . Ceq2 is the equivalent capacitance with Cc , Co , Cr and Cc/n2 in series. However for a well-designed converter, the capacitance of Cc and Co is normally much higher than Cr , so we have Ceq2 ≈ Cr . t7 –t8 : At t8 , iDo resonates to zero, Do turns off with ZCS. From t5 to t8 ,the voltage applied on Lm is Vin –VC c , which decreases iLm to a negative valley to provide a ZVS turn-on condition of S1 . iLm within t5 –t8 can be calculated by

$$i_{L_m}(t) = i_{L_m}(t_5) + \frac{V_{in} - V_{Cc}}{L_m}(t - t_5) \qquad (10)$$

Assuming the switching transition periods of t0 –t1 and t4 –t5 are negligibly short, the boost ratio Mb can be derived by three flux balance criteria in the steady state. The first flux balance equation which governs the circuit is from the flux balance of Lm during the whole switching period. This can be obtained from (5) and (10) as

$$\int_0^{T_s} L_m i_{L_m}(t)dt = \int_{t_1}^{t_4} V_{in}dt + \int_{t_5}^{t_8}(V_{in} - V_{Cc})dt$$
$$= \int_0^{DT_s} V_{in}dt + \int_{DT_s}^{T_s}(V_{in} - V_{Cc})dt = 0 \qquad (11)$$

Second flux balance equation can be derived from (3) according to flux balance on Llk within the period t1 – t3

$$\int_{t_1}^{t_3} L_{lk}i_{Cr}(t)dt$$
$$= \int_{t_1}^{t_3} L_{lk}\frac{nV_{in} + V_{Cc} - v_{Cr}(t_1)}{Z_{r1}}\sin\omega_{r1}(t - t_1)dt = 0 \qquad (12)$$

TABLE:I:SPECIFICATION AND POWER STAGE PARAMETERS

Converter	ACCI converter	Proposed converter
Rated power	250 W	250 W
Output voltage	380 V	380 V
Input voltage range	20–45 V	20–45 V
Output power range	25W~250 W	25W~250 W
Turns ratio	$n_1 = 70/3$	$n_2 = 16/3$
Switching frequency	100 kHz	100 kHz
Magnetizing inductor	$L_{m1} = 20\,\mu H$	$L_{m2} = 5.6\,\mu H$
Clamping capacitor	$C_c = 20\,\mu F$	$C_c = 20\,\mu F$
External inductor	$L_{ex} = 1\,\mu H$	N.A.
Resonant capacitor	NA	$C_r = 0.40\,\mu F$
R-C snubber	Yes	N.A.

Similarly, the last flux balance can be derived from (8) according to flux balance on Llk within the period t5 – t7

$$\int_{t_5}^{t_7} L_{lk} i_{Cr}(t)dt = \int_{t_5}^{t_7} L_{lk} \frac{nV_{in} - (n+1)V_{Cc} + V_o - v_{Cr}(t_5)}{Z_{r2}}$$
$$\times \sin\omega_{r2}(t - t_5)dt = 0 \qquad (13)$$

Normally, the ripple voltage on Cr is small compared to the average voltage VC r of Cr . Replacing VC r into (12) and (13) and solving (11), (12) and (13) yields

$$M_b = \frac{V_o}{V_{in}} = \frac{n+2}{1-D} \qquad (14)$$

$$V_{Cr} = \frac{n+1-D\cdot n}{n+2}V_o \qquad (15)$$

$$V_{Cc} = \frac{V_{in}}{1-D} = \frac{V_o}{n+2} \qquad (16)$$

Equation (14) reveals that the conversion ratio of the proposed converter is similar to the conventional boost converter except for additional n + 1 gain boost. This boost gain feature is very beneficial to implement an inner voltage control loop inside the maximum power point tracking (MPPT) loop to reject the double-line-current from the following-stage single-phase inverter since it is like a buck converter from the output to input [4], [5].

PROPOSED CONCEPT ADVANTAGES

The advantages of the proposed converter are analyzed in this section to highlight its suitability for PV module applications. The specifications of PV module used for the analysis in this section and for system experimental verification is CS6P-240P [9] from CanadianSolar. In order to demonstrate the improvements of introducing resonant operation into traditional PWM converters, the high boost ratio ACCI converter in [19] and the proposed converter will be comparatively analyzed. The specification requirements and the parameters of two prototype converters are shown in Table I.

DESIGN IMPLEMENTATION:

For the following analysis, the notations with subscripts 1 and 2 represent ACCI converter in [19] and the proposed converter respectively.
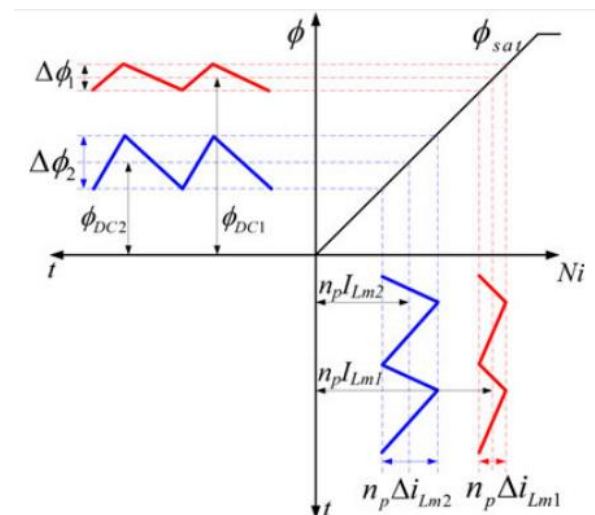

Fig.Total flux in the magnetic core versus MMF:

EXPERIMENTALVERIFICATIONS:

The implementation experiment, the prototype converter was designedto convert the low input voltage Vin from PV module with thevoltage varying from 20 to 45 V to a constant high dc-busvoltage 380 V. To achieve final low profile design, we designthe transformer with low profile magnetic core RM14-LP.Dueto the increased boost gain as calculated in (14) as comparedto traditional coupled-inductor based PWM converters, we candecrease the turns ratio of the transformer, allowing optimalutilization of the window area of the magnetic core. This isbeneficial to low-profile type cores, since they normally havesmaller window area compared to the regular counterparts.Fig.

8 highlights the experimental waveforms of driver signalofS1, input current ip and drain–source voltage ofS1 withVin =30 V,Po =220 W andVo =380 V.

As seen from Fig. 8,the switch voltage stress is kept at a low level; the input currentis composed of sinusoidal resonant and linear PWM currents,illustrating hybrid resonant and PWM power conversion. Thishybrid operation improves the utilization of magnetics. Theresonant portion of the primary current resonates back to zeroat both on and off periods of the main switch. This helps ZCSturn-off of both resonant and output diodes. WhenS1turns off,the primary side current is at the peak point, which helps S2achieving ZVS turn on. However whenS1turns on, the primaryside current is at the valley point, which helpsS1achieving ZVSturn on.Fig. 9 shows the zoom-in waveforms indicating ZVS of mainswitchS1. It can be seen when S1 is turned, the drain–sourcevoltage ofS1 has reached to zero, illustrating the ZVS turn on of S1.Fig. 10 shows the zoom-in waveforms indicating ZVS ofauxiliary switchS2. It can be seen that main switchS1is turnedoff by the driverg1within the "Miller Plateau." With the positivecurrentip,S2can be turned on with ZVS after dead time.

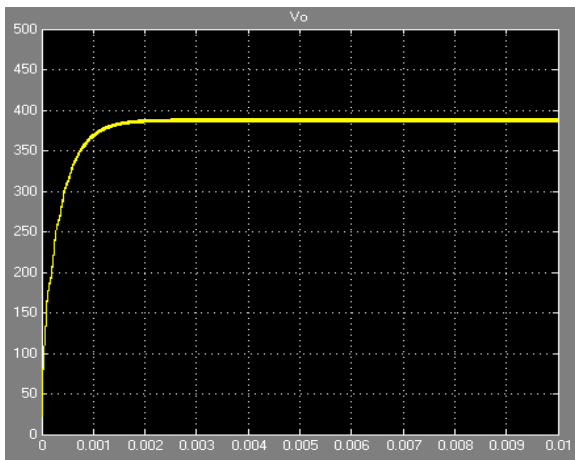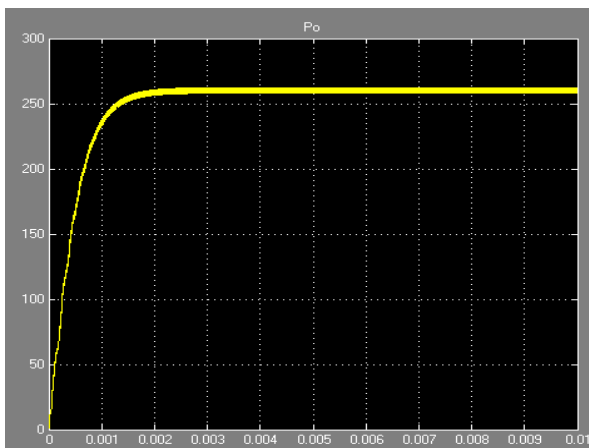## SIMULINK RESULTS AND OUTPUTS
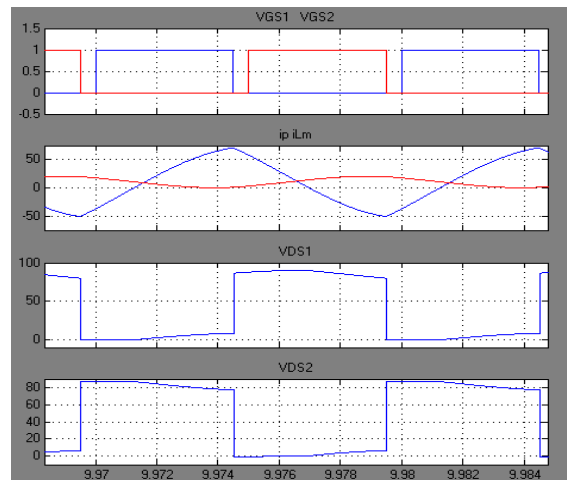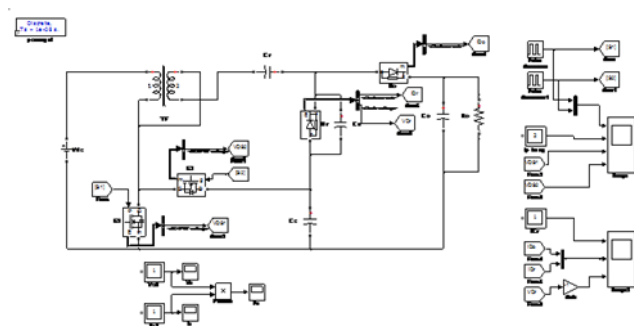
Output waveform of the
a) Gate pluse VGS1&2
b) Transformer pir current &Lm current
c) Diode voltage 1& d)2
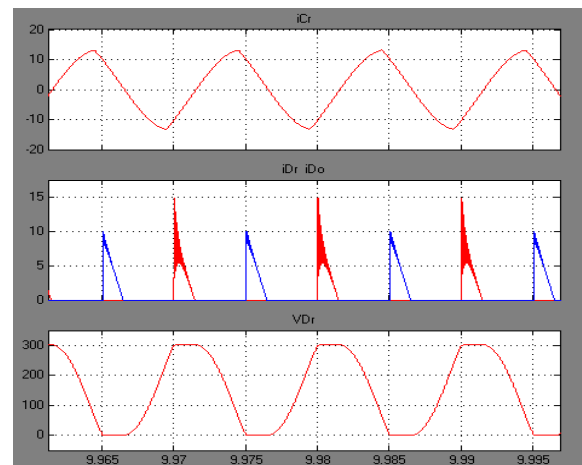
Output waveform of the
 a) **Capacitor Cr current**
 b) **Diode Dr,D0 current**
 c) **Diode Dr voltage**

Output voltage

Output power:

CONCLUSIONS:

By incorporating resonant operation mode into traditional high boost ratio activeclamp coupled-inductor PWM converter, a high boost ratio ZVS/ZCS PV module integrated dc–dc converter with hybrid transformer is presented.

A) ZVS turn-on of active switches and ZCS turn-off ofdiodes, reducing the switching losses and EMI noises;

B) fixed low voltage stresses for all power devices at steadystate operations, independent of wide changing input PVmodule voltage;

C) the MU is optimized as a result of energy transfer to thehigh voltage side throughout the whole switching period,allowing utilization of smaller-size magnetics and lowprofile design;

D) continuous input current with combined resonant andPWM waveforms reducing the RMS conduction losses;

E) flat efficiency curves leading to high CEC efficiency over wide input voltage range;

F) elimination of lossysnubber circuit for output diodes;

G) although an additional resonant diode and a small resonantcapacitor are added, the total PDU is improved;

H) the input voltage region with high CEC efficienciesmatches the PV module maximum power point ranges, achieving maximum energy yield.

A prototype circuit targeted for PV module integration with20–45 V input voltage range and 380 V dc output was builtand tested. The test CEC efficiencies including the driver andauxiliary power supply losses are higher than 96.7% from20 to 45 V input voltages. Due to the simple structure, easytocontrol, low profile design and high CEC efficiency over wide input voltage and output power ranges, the proposed converter is very attractive to work as a PV module integrated converter.

REFERENCES:

[1] M. H. Nehir, C. Wang, and S. R. Guda, "Alternative energy distributedgeneration: Need for multi-source operation," in Proc. North Amer. PowerSymp., 2006, pp. 547–551.

[2] T. J. Hammons, J. C. Boyer, S. R. Conners,M. Davies,M. Ellis,M. Fraser,E. Holt, and J. Markard, "Renewable energy alternatives for developedcountries," IEEE Trans. Energy Convers., vol. 15, no. 4, pp. 481–493,Dec. 2000.

[3] P. K. KattiandM. K. Khedkar, "Fostering the use of low impact renewableenergy technologies with integrated operation is the key for sustainableenergy system," in Proc. Joint Int. Conf. Power Syst. Technol. IEEE PowerIndia, 2008, pp. 1–8.

[4] J. L. Sawin. (2014, Aug. 13). Renewables 2013 - Global StatusReport.[Online].

Available:http://www.ren21.net/portals/0/documents/resources/gsr/2013/gsr2013_lowres.pdf

[5] U. K. Madawala, D. J. Thrimawithana, X. Dai, and D. M. Vilathgamuwa,"A model for a multi-sourced green energy system," in Proc. IEEE Conf.Sustainable Energy Technol., 2010, pp. 1–6.

[6] J. Marsden, "Distributed generation systems: A new paradigm for sustainableenergy," in Proc. IEEE Green Technol., 2011, pp. 1–4.

[7] R. Ramakumar and P. Chiradeja, "Distributed generation and renewableenergy systems," in Proc. 37th Intersoc.Energy Convers. Eng. Conf. ,2002, pp. 716–724.

[8] S. I. Mustapa, Y. P. Leong, and A. H. Hashim, "Issues and challengesof renewable energy development: A Malaysian experience," inProc. Int. Conf. Energy Sustainable Develop.: Issues Strategies, 2010,pp. 1–6.

[9] W. Kempton and S. Letendre, "Electric vehicles as a new power sourcefor electric utilities," Transp. Res. Part D, Transport Environ., vol. 2,pp. 157–175, 1997.

[10] B. Kramer, S. Chakraborty, and B. Kroposki, "A review of plug-in vehiclesand vehicle-to-grid capability," in Proc. IEEE Ind. Electron., 2008,pp. 2278–2283.

[11] U. K. Madawala, P. Schweizer, and V. V. Haerri, ""Living and mobility"—A novel multipurpose in-house grid interface with plug-in hybridblue angel," in Proc. IEEE Conf. Sustainable Energy Technol., 2008,pp. 531–536.

[12] U. K. Madawala and D. J. Thrimawithana, "A bidirectional inductivepower interface for electric vehicles in V2G systems," IEEE Trans. Ind.Electron., vol. 58, no. 10, pp. 4789–4796, Oct.2011.

[13] D. J. Thrimawithana, U. K. Madawala, R. Twiname, and D. M. Vilathgamuwa,"A novel matrix converter based resonant dual active bridge forV2Gapplications," in Proc. IPEC Conf. Power Energy, 2012, pp. 503–508.

[14] D. C. Erb, O. C. Onar, and A. Khaligh, "An integrated bi-directionalpower electronic converter with multi-level AC-DC/DC-AC converterand non-inverted buck-boost converter for PHEVs with minimal gridlevel disruptions," in Proc. IEEE Vehicle Power Propulsion Conf., 2010,pp. 1–6.

[15] R. L. Steigerwald, R.W.DeDoncker, andH.Kheraluwala, "A comparisonof high-power DC-DC soft-switched converter topologies," IEEE Trans.Ind. Appl., vol. 32, no. 5, pp. 1139–1145, Sep./Oct. 1996.